Phys. Rev. 119, 1025 (1960).

[8]J. C. Slater, *Quantum Theory of Molecules and Solids*, Vol. 1 (McGraw-Hill, New York, 1963), p. 17.

[9]G. Wentzel, Z. Phys. 27, 257 (1924); for a discussion see L. C. Biedenharn and P. J. Brusaard, *Coulomb Excitation* (Clarendon Press, Oxford, 1965), pp. 31–40.

[10]R. S. Berry, J. Chem. Phys. 45, 1228 (1966).

[11]J. N. Bardsley, Chem. Phys. Letters 1, 229 (1967).

[12]A. Russek, M. R. Patterson, and R. L. Becker,

Phys. Rev. 167, 17 (1968).

[13]As an example of this form of wave function used in ion-atom charge transfer reactions see D. F. Gallaher and L. Wilets, Phys. Rev. 169, 139 (1968).

[14]D. R. Bates, *Quantum Theory. Elements* 1 (Academic, New York, 1961), pp. 251–297.

[15]L. D. Landau and E. M. Lifshitz, *Quantum Mechanics* (Addison-Wesley, Reading, Mass., 1958), Sec. 36.

Exact Screened Calculations of Atomic-Field Bremsstrahlung*

H. K. Tseng and R. H. Pratt

Department of Physics, University of Pittsburgh, Pittsburgh, Pennsylvania 15213

(Received 16 July 1970)

A discussion of relativistic bremsstrahlung cross sections is given for incident-electron kinetic energies in the range 5 keV–1 MeV, based on an exact numerical calculation using screened potentials. Comparisons are made with previous authors' results, extending the discussion of a preliminary note. Exact point-Coulomb and Born-approximation results are contrasted. The present results show that the Born approximation significantly underestimates the bremsstrahlung cross sections in the energy region considered. Screening effects are somewhat larger than expected, and when large are not well described by a form factor.

I. INTRODUCTION

The exact calculation of relativistic atomic-field electron bremsstrahlung beyond the Born approximation (the well-known Bethe-Heitler formula[1]) has been possible only in certain limiting cases. Results have been obtained for extreme relativistic energies by Bethe, Maximon, Olsen, and others[2] using analytic approximate high-energy electron wave functions. In the nonrelativistic case, calculations were made by Sommerfeld, Elwert, and others[3] for the point-Coulomb field, neglecting screening. A gap has remained in the theory for intermediate energies (kinetic energy of the incident electron $T_1 \equiv E_1 - m_e c^2 = 5$ keV–50 MeV), except for those cases in which Born approximation is valid. The purpose of this work[4] is to obtain information regarding the bremsstrahlung cross sections at these intermediate energies by making a direct numerical calculation. Even with modern computers, it is not yet feasible to perform comprehensive calculations covering this entire energy region. But it is possible to establish the importance of Coulomb corrections to the Born approximation and the importance of electron-screening corrections to point-Coulomb results. It is also possible to formulate analytical expressions useful at high and low energies. Hopefully, the results we have obtained can serve also as reference points in the construction of better approximate theories.

While this work was in progress Brysk, Zerby,

and Penny (BZP)[5] reported a similar numerical calculation and Elwert and Haug (EH)[6] used approximate electron wave functions to obtain analytic results valid (neglecting screening) for all energies, at least for low-Z elements. We have already commented on this work in a preliminary note,[7] showing that BZP angular distributions are incorrect and EH results are poor for large Z. Further analysis of these papers will be given below.

We wish here to present a more complete discussion of the calculation of relativistic bremsstrahlung cross sections for incident-electron kinetic energies in the range 5 keV–1 MeV. Our methods are similar to those used by Schmickley and Pratt[8] in the calculation of atomic photoeffect, and are based on the description of the atom as a static spherically symmetric charge distribution of infinite
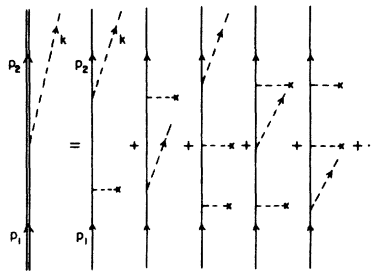
FIG. 1. Furry diagram (left) and Feynman diagrams (right) for Bremsstrahlung.

TABLE I. Bremsstrahlung cross sections σ(k) as computed in this work. Symbols B, C, S, HFS, TFC, and TF refer to the Born approximations, point-Coulomb, screened, modified Hartree-Fock-Slater, modified Thomas-Fermi, and Thomas-Fermi potentials; and n_{κ_1} and n_{κ_2} are the number of κ_1's and of κ_2's used in this work, respectively.

| Z | T_1 | k | $\sigma^B(k)$ | $\sigma^C(k)$ | $\sigma^S(k)$ (mb) | | | | | | Fig. |
	(MeV)	(MeV)	(mb)	(mb)	HFS	TFC	TF	γ_β	n_{κ_1}	n_{κ_2}	numbers
1	0.380	0.228	4.477	4.513	•••	•••	•••	0.072	36	22	2
1	0.500	0.480	0.8043	0.8549	•••	•••	•••	0.17	28	8	14
1	0.500	0.250	4.984	4.985	•••	•••	•••	0.062	48	30	3
8	0.045	0.040	12.10	22.78	•••	•••	•••	2.6	14	8	5
13	0.005	0.004	152.0	335.2	295.7	288.2	283.4	9.6	18	16	4
13	0.045	0.040	12.10	28.03	27.63	•••	•••	4.3	14	8	5
13	0.050	0.040	15.28	26.77	26.30	26.03	•••	3.1	16	12	6
13	0.050	0.030	24.27	32.57	31.76	31.43	•••	2.2	24	20	7
13	0.050	0.020	34.46	40.34	38.73	•••	•••	1.8	36	32	8
13	0.500	0.480	0.8043	1.531	•••	•••	•••	2.2	28	8	14
13	1.000	0.700	2.590	2.901	2.892	•••	•••	0.77	66	28	16
79	0.050	0.030	24.27	42.59	35.62	36.17	•••	13.	24	20	9
79	0.050	0.020	34.46	46.72	37.29	•••	•••	11.	36	32	10
79	$0.25\,m_ec^2$	$0.1875\,m_ec^2$	7.130	17.74	16.03	•••	•••	11.	24	14	11
79	0.180	0.108	7.551	14.67	13.34	•••	•••	7.5	30	22	12
79	0.380	0.228	4.477	8.522	7.942	•••	•••	5.7	36	22	13
79	0.500	0.480	0.8043	4.789	4.526	•••	•••	13.	28	8	14
79	0.500	0.250	4.984	8.142	7.600	•••	•••	4.9	48	30	15

mass. As in BZP, the electron wave functions are calculated in partial wave series, and radial matrix elements are obtained by a numerical integration over numerically obtained radial wave functions. In Sec. II we give a brief survey of bremsstrahlung theory and in Sec. III we discuss our numerical methods. Comparisons with previous results, both theory and experiment, are presented in Sec. IV.

We also there use our results to examine Coulomb corrections and screening effects. We compare the present Coulomb-correction values with the Elwert factor, [6] and the present screening values with the form-factor results obtained using Born approximation theory. [9]
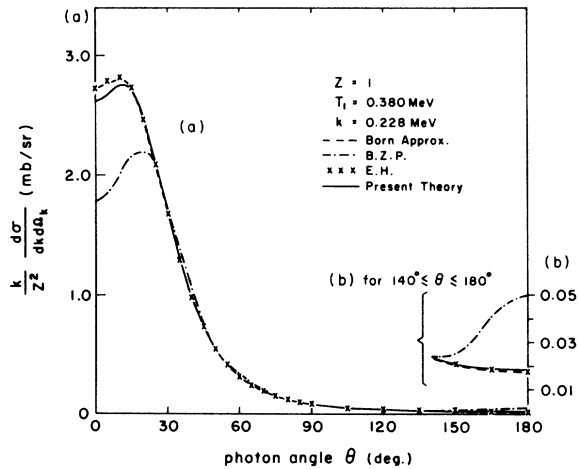
FIG. 2. Bremsstrahlung differential cross sections σ(k, θ) for Z = 1, T_1 = 0.380 MeV, k = 0.228 MeV. (For θ ≳ 15° our results are larger than the Born-approximation results and the integrated cross section σ(k) is dominated by the region 60° > θ > 10°, the sinθ in $d\Omega_k$ diminishing the contribution of the small θ region where our results are smaller than the Born approximation.)
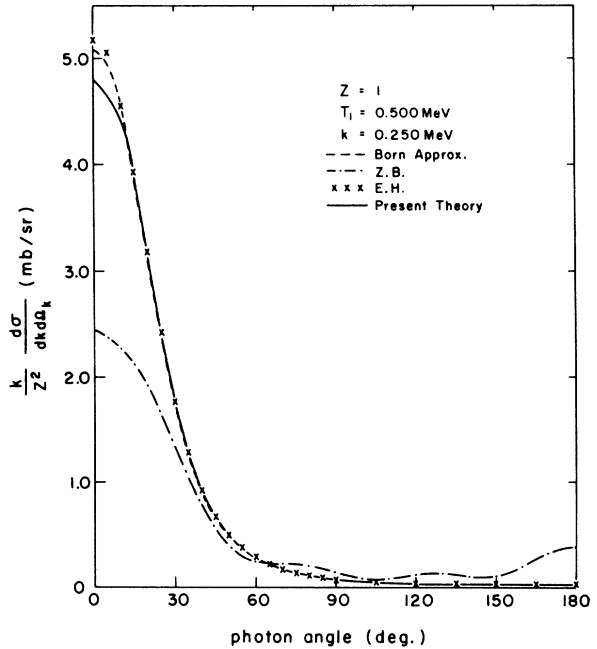
FIG. 3. Bremsstrahlung differential cross sections σ(k, θ) for Z = 1, T_1 = 0.500 MeV, k = 0.250 MeV.
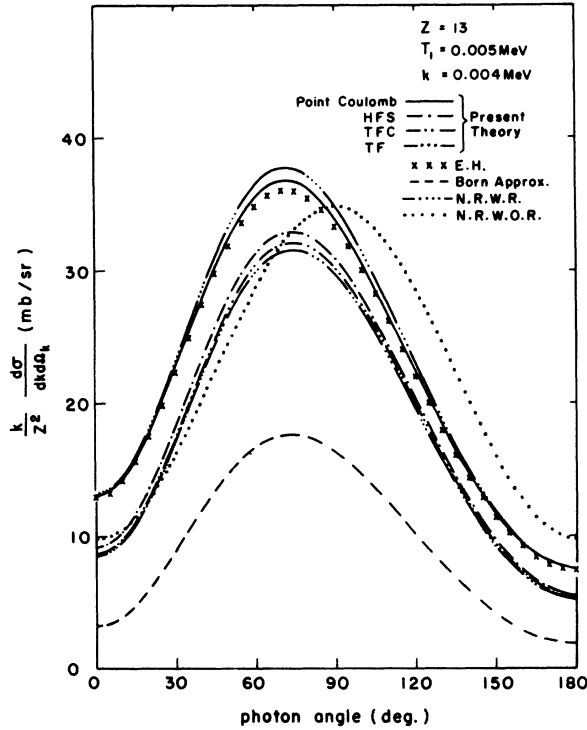
FIG. 4. Comparison of present results of Brems-
strahlung differential cross sections $\sigma(k, \theta)$ (solid line
for point-Coulomb, dotted-broken line for HFS field,
double-dotted-broken line for TFC field, and triple-
dotted-broken line for TF field) with the Born-approxi-
mation results (broken line), the results of EH (crosses),
and the nonrelativistic results [dotted line for results
without retardation (N.R.W.O.R.), quadruple-dotted
broken line for results with retardation (N.R.W.R.)]
for the case $Z = 13$, $T_1 = 0.005$ MeV, $k = 0.004$ MeV.

II. THEORY

Our formalism corresponds to Furry's extension[10]
of the usual Feynman-Dyson formulation[11] of quan-
tum electrodynamics, including the interaction of
the electrons with the atomic field in the unper-
turbed Hamiltonian. The bremsstrahlung process
is shown symbolically in Fig. 1. The right-hand
and left-hand sides are Feynman and Furry dia-
grams, respectively. The diagrams corresponding
to radiative corrections are neglected in our ap-
proximation as this correction is quite small in the
energy region we consider here. (The lowest-or-
der radiative corrections to the bremsstrahlung
cross sections were obtained by Fomin. [12])

The (incoming and outgoing) electrons in the
atomic field and the photons are described by oper-
ators $\Psi(x)$ and $A^{\text{rad}}(x)$, respectively, which satisfy
the equations

$$(i\not{\partial} - e\not{A}^{\text{Coul}} - 1)\Psi(x) = 0 , \qquad (2.1)$$

$$\Box A^{\text{rad}}(x) = 0 , \qquad (2.2)$$

where A^{Coul} is the vector potential describing the
atomic field. The solution of (2.1) and (2.2) is
written as[13]

$$\Psi(x) = \sum_{\vec{p}, s} [\Psi^{(+)}(\vec{p}, s) e^{-iEt} b(\vec{p}, s)$$

$$+ \Psi^{(-)}(\vec{p}, s) e^{iEt} d^\dagger(\vec{p}, s)] ,$$

$$A_0^{\text{rad}} = 0 , \qquad (2.3)$$

$$\vec{A}^{\text{rad}}(x) = \left(\frac{2\pi}{k}\right)^{1/2} \sum_{\vec{k}, \vec{\epsilon}} [e^{-ikx} \vec{\epsilon} a(\vec{k}, \vec{\epsilon}) + e^{ikx} \vec{\epsilon}^* a^\dagger(\vec{k}, \vec{\epsilon})] ,$$

where b and $d^\dagger$ are annihilation and creation opera-
tors for electrons and positrons, respectively; a
and $a^\dagger$ are destruction and creation operators for
photons, specified by four-momentum $(k, \vec{k})$ and
four-polarization $(0, \vec{\epsilon})$. Here the radiation gauge
was chosen. Although we lose manifest Lorentz
and gauge covariance, only the two transverse de-
grees of freedom of the radiation field appear in
the formalism. The cross sections in this approx-
imation are obtained from the matrix element of
the S matrix between the initial and final states

$$S_{fi} = \langle p_2 k | S | p_1 \rangle$$
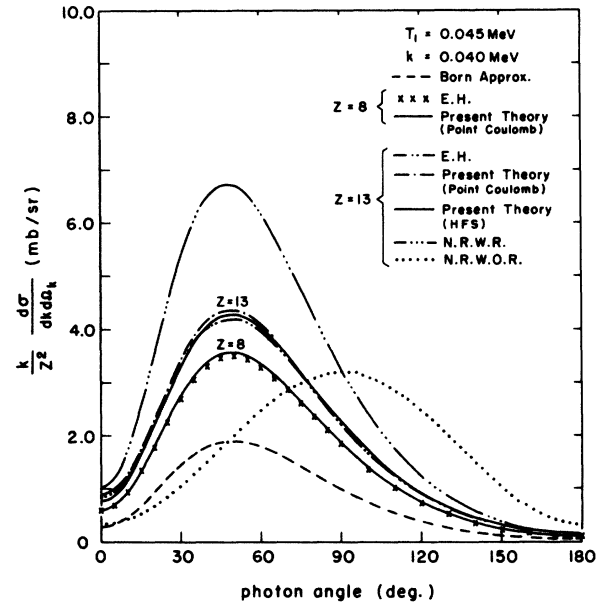
FIG. 5. Bremsstrahlung differential cross sections
$\sigma(k, \theta)$ of present theory (solid line for $Z = 8$ point-Cou-
lomb field, single-dotted-broken line and solid line for
$Z = 13$ point-Coulomb field and HFS field, respectively)
for the cases $T_1 = 0.045$ MeV, $k = 0.040$ MeV, with $Z = 8$
and $Z = 13$, compared with the Born-approximation re-
sults (broken line), the nonrelativistic results for $Z = 13$
(dotted line for N.R.W.O.R., triple-dotted-broken line
for N.R.W.R.), and those of EH (crosses for $Z = 8$,
double-dotted-broken line for $Z = 13$).
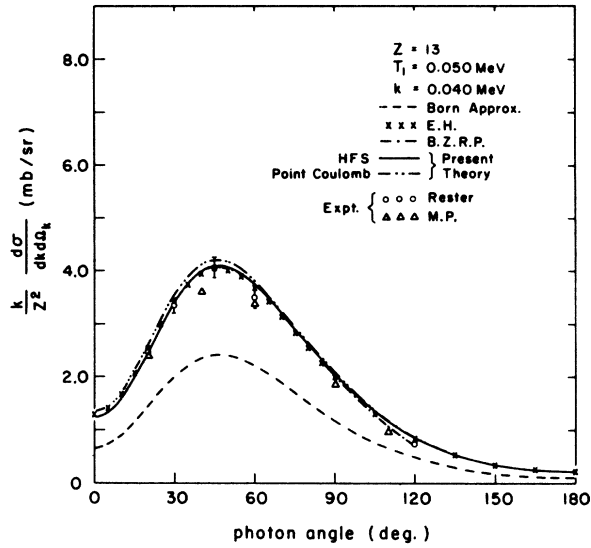
FIG. 6. Comparisons of present results (solid line for HFS field, double-dotted-broken line for point-Coulomb field) with the Born-approximation results (broken line), the results of BZRP (dotted-broken line), the results of EH (crosses), and the experimental data of MP (triangles) and of Rester (circles) for the case $Z = 13$, $T_1 = 0.050$ MeV, $k = 0.040$ MeV.

$$\cong \langle p_2 k \,|\, 1 - ie \int d^4 x : \bar{\Psi}(x) \mathcal{A}^{\mathrm{rad}}(x) \Psi(x) : \,|\, p_1 \rangle$$

$$= ie \,(2\pi/k)^{1/2} \int d^4 x \psi_2^\dagger \vec{\alpha} \cdot \vec{\epsilon}^* \,\psi_1 \, e^{-i\vec{k}\cdot\vec{r}} \, e^{-i(E_1 - E_2 - k)t}$$
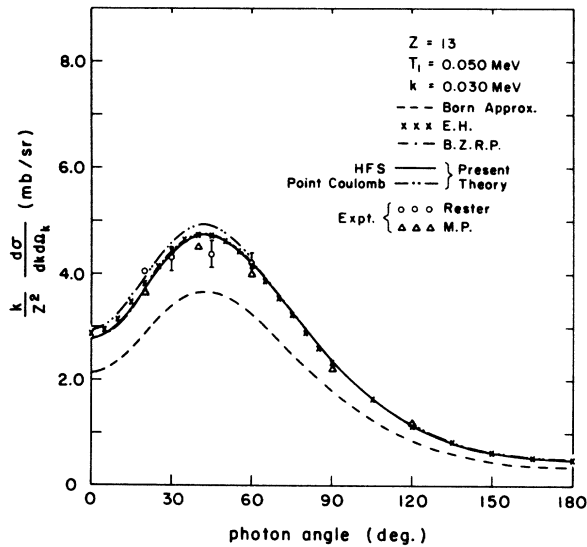
FIG. 7. Comparison of present results (solid line for HFS field, double-dotted-broken line for point-Coulomb field) with the Born-approximation results (broken line), the results of BZRP (dotted-broken line), the results of EH (crosses), and the experimental data of MP (triangles) and of Rester (circles) for the case $Z = 13$, $T_1 = 0.050$ MeV, $k = 0.030$ MeV.

$$= -i \, 2\pi M_{fi} \, \delta(E_1 - E_2 - k) \ . \tag{2.4}$$

Here

$$M_{fi} = (2\pi\alpha/k)^{1/2} \int d^3 r \psi_2^\dagger \vec{\alpha} \cdot \vec{\epsilon}^* \,\psi_1 \, e^{-i\vec{k}\cdot\vec{r}} \ ;$$

$$\vec{\alpha} = \begin{pmatrix} 0 & \vec{\sigma} \\ \vec{\sigma} & 0 \end{pmatrix} \ ,$$

$\vec{\sigma}$ are the familiar 2×2 Pauli matrices; ψ_1 is the initial wave function asymptotically normalized to a unit-amplitude modified plane wave of four-momentum $(E_1, \vec{p}_1)$ plus an outgoing spherical wave; and ψ_2 is the final wave function asymptotically normalized to a unit-amplitude modified plane wave of four-momentum $(E_2, \vec{p}_2)$ plus an incoming spherical wave.[14] The transition probability per unit time between the states is then

$$W_{fi} = 2\pi \,|M_{fi}|^2 \, \delta(E_1 - E_2 - k) \ ,$$

from which we can obtain the cross section by summing over the energies of the final state and dividing by the flux of incoming particles (in this case the velocity of the incident electron v_1 relative to
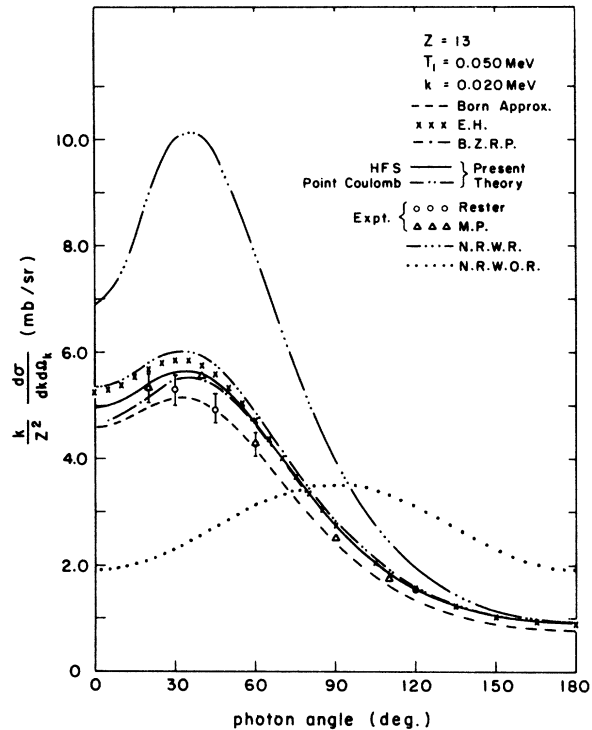
FIG. 8. Comparison of present results (solid line for HFS field, double-dotted-broken line for point-Coulomb field) with the Born-approximation results (broken line), the results of BZRP (dotted-broken line), the results of EH (crosses), the experimental data of MP (triangles) and of Rester (circles), and the nonrelativistic results (dotted line for N.R.W.O.R., triple-dotted-broken line for N.R.W.R.) for the case $Z = 13$, $T_1 = 0.050$ MeV, $k = 0.020$ MeV.
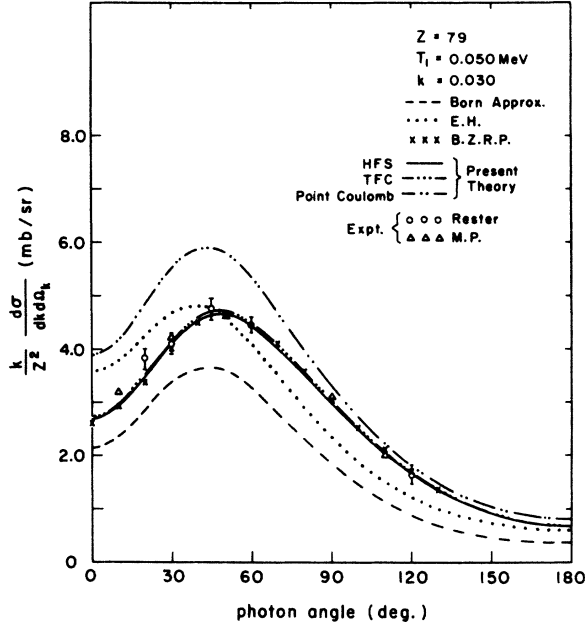
FIG. 9. Comparisons of present results (solid line for HFS field, double-dotted-broken line for point-Coulomb field, and triple-dotted-broken line for TFC field) with the Born-approximation results (broken line), the results of BZRP (crosses), the results of EH (dotted line), and the experimental results of MP (triangles) and of Rester (circles) for the case $Z = 79$, $T_1 = 0.050$ MeV, $k = 0.030$ MeV.

the atom). Since the density of final states is given by

$$\rho_F = \rho(\vec{p}_2)\,\rho(\vec{k})\,dk\,dE_2 \ ,$$

where

$$\rho(\vec{p}_2) = p_2 E_2\, d\,\Omega_2/(2\pi)^3, \quad \rho(\vec{k}) = k^2\, d\Omega_k/(2\pi)^3 \ ,$$

we obtain the cross section, after integration over energies E_2 of the outgoing electron,

$$d\sigma = (2\pi)^{-5}\,(E_1 p_2 E_2 k^2/p_1)\,dk\,d\Omega_k\,d\Omega_2\,\big|M_{fi}\big|^2 \ . \qquad (2.5)$$

We use the split representation; in this way any matrix element between four-component states may be reduced to matrix elements between two-component spinors

$$\chi = \sum_s a_s \chi^s, \text{ with } \chi^\dagger \chi = 1, \ \chi^{1/2} = \begin{pmatrix} 1 \\ 0 \end{pmatrix}, \ \chi^{-1/2} = \begin{pmatrix} 0 \\ 1 \end{pmatrix} \ .$$

This gives a simple method to separate out the quantities depending on polarization. Since

$$[\vec{J}, H] = 0 \ ,$$

where we have the angular momentum operator

$$\vec{J} = \vec{L} + \vec{S} = \vec{r} \times \vec{p} + \tfrac{1}{2}\vec{\sigma}$$

and the Hamiltonian

$$H = -i\,\vec{\alpha}\cdot\vec{\nabla} + \beta + V(r) \qquad\qquad [\,V(r) = eA_0^{\text{cou}1}\,],$$

we may construct simultaneous eigenfunctions of H, J^2, J_z and the parity operator βI_S, where I_S is the space-inversion operator, since $[\beta I_S, H] = 0$ too. Thus we have[15]

$$\psi_{\text{out}}^{\text{in}}(\vec{p}, \vec{r}, \vec{\zeta}) = 4\pi \sum_{\kappa m} [\Phi_{\kappa m}^\dagger(\hat{p})\,\chi(\vec{\zeta})]\,i^{l-1}\,e^{\mp i\delta_\kappa}\,\psi_{\kappa m}(\vec{r}) \ ,$$

where

$$\psi_{\kappa m}(\vec{r}) = \begin{pmatrix} ig_\kappa(r)\,\Phi_{\kappa m}(\hat{r}) \\ -f_\kappa(r)\,\Phi_{-\kappa m}(\hat{r}) \end{pmatrix}\Big/ r$$

and

$$\Phi_{\kappa m}(\hat{r}) = \sum_s C(l\tfrac{1}{2}j\,;\,m-s,\,s)\,Y_{l,m-s}(\hat{r})\,\chi^s \ ,$$

an eigenstate of $\vec{J}^2$ and $\vec{L}^2$,

$$\begin{pmatrix} \vec{J}^2 \\ J_z \\ \vec{L}^2 \\ \vec{S}^2 \end{pmatrix} \Phi_{\kappa m} = \begin{pmatrix} j(j+1) \\ m \\ l(l+1) \\ s(s+1) \end{pmatrix} \Phi_{\kappa m} \ .$$
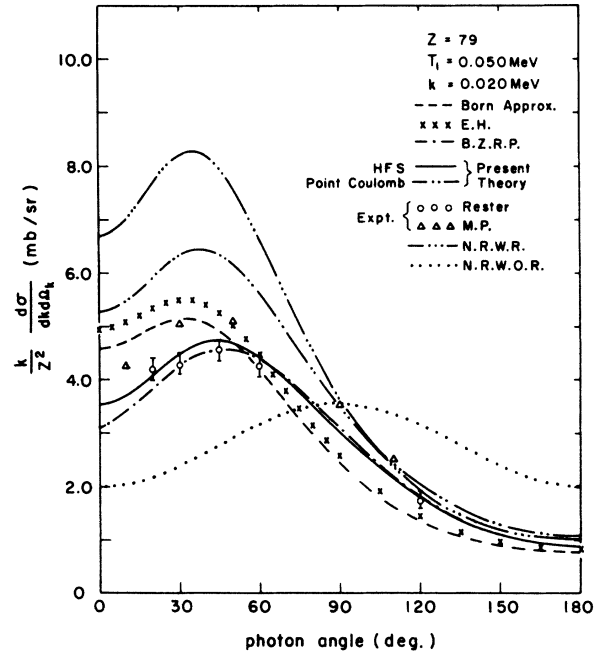
FIG. 10. Comparisons of present results (solid line for HFS field, double-dotted-broken line for point-Coulomb field) with the Born-approximation results (broken line), the results of BZRP (single-dotted-broken line), the results of EH (crosses), the experimental data of MP (triangles) and of Rester (circles), and the nonrelativistic results (dotted line for N. R. W. O. R., triple-dotted-broken line for N. R. W. R.) for the case $Z = 79$. $T_1 = 0.050$ MeV, $k = 0.020$ MeV.
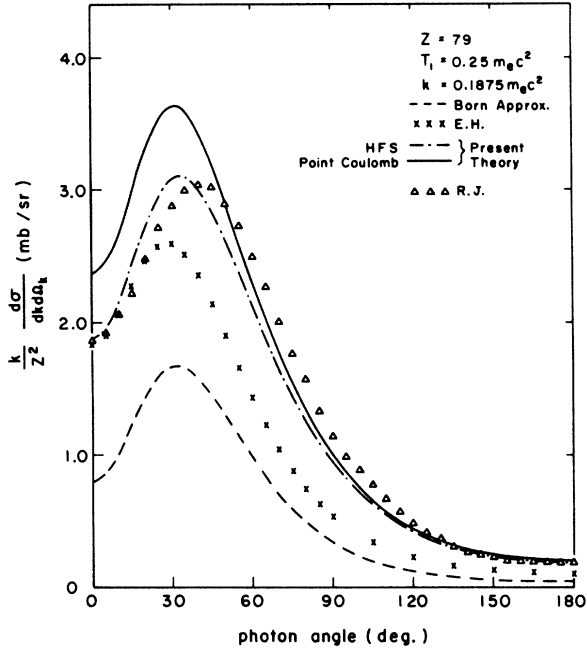
FIG. 11. Bremsstrahlung differential cross sections $\sigma(k,\theta)$ of present theory (solid line for point Coulomb field, dotted broken line for HFS field) for the case $Z=79$, $T_1=0.25\ m_ec^2$, $k=0.1875\ m_ec^2$, compared with the Born-approximation results (broken line), the results of EH (crosses), and the results of RJ (triangles).

Also, we have

$$K\Phi_{\kappa m} \equiv (\vec{\sigma}\cdot\vec{L}+1)\,\Phi_{\kappa m} = -\kappa\,\phi_{\kappa m}\ ;$$

$$\kappa = \mp(j+\tfrac{1}{2})\ \text{as}\ j=l\pm\tfrac{1}{2}\ .$$

The radial wave functions g_κ and f_κ satisfy the equations

$$\frac{dg}{dr} = (E+1-V)f - \frac{\kappa g}{r}\ ,$$

$$\frac{df}{dr} = -(E-1-V)g + \frac{\kappa f}{r}\ ,$$

$$(2.7)$$

where V is the screened central potential for the atomic electron in question.

Choosing a coordinate system centered at the atomic nucleus with the z axis along $\vec{k}$, $\hat{y}$ along $\vec{k}$ $\times\vec{p}_1$, and $\hat{x}$ in the $(\vec{k},\ \vec{p}_1)$ plane, and inserting Eq. (2.6) into Eq. (2.4), we obtain[4,16]

$$M_{fi} = 16\pi^2\left(\frac{2\pi\alpha}{k}\right)^{1/2}\sum_{\kappa_1 m_1 \kappa_2 m_2}\ [\ \Phi_2^\dagger(\hat{p}_2)\,\chi_2]^\dagger\ [\ \Phi_1^\dagger(\hat{p}_1)\,\chi_1]$$

$$\times(-)^{l_1}e^{i(\delta_{\kappa_1}+\delta_{\kappa_2})}\left[\epsilon_+^* R_+(m_2)+\epsilon_-^* R_-(m_2)\right]\ ,$$

where

$$(2.8)$$

$$\epsilon_\pm \equiv \epsilon_x\pm i\epsilon_y\ ,$$

$$R_\pm(m_2) = \delta_{m_1,\,m_2\mp1}\sum_{n=1}^{2}Q_n^\pm(m_2){\sum_l}'P_n^\pm(m_2)S_n\ .\quad(2.9)$$

The index l runs from $|l_2'-l_1|$ to $(l_2'+l_1)$ in steps of 2 for $n=1$, and from $|l_2-l_1'|$ to (l_2+l_1') in steps of 2 for $n=2$:

$$l'\equiv l+\eta_\kappa\ ,\quad \eta_\kappa\equiv -\kappa/|\kappa|\ ;$$

$$Q_1^\pm(m) = \eta_{\kappa_2}(-)^{m\mp1/2}[(2l_2'+1)(2l_1+1)]^{1/2}C_{2'}^\pm C_1^\mp\ ,$$

$$Q_2^\pm(m) = -\eta_{\kappa_1}(-)^{m\mp1/2}[(2l_2+1)(2l_1'+1)]^{1/2}C_2^\pm C_{1'}^\mp\ ,$$

$$P_1^\pm(m) = (-)^{(l_2'+l_1+l)/2}T(l_2',\ l_1,\ l;\ m\mp\tfrac{1}{2})\ ,$$

$$P_2^\pm(m) = (-)^{(l_2+l_1'+l)/2}T(l_2,\ l_1',\ l;\ m\mp\tfrac{1}{2})\ ,$$

$$T(l_2,\ l_1,\ l;\ m)\equiv(2l+1)\begin{pmatrix}l_2&l_1&l\\0&0&0\end{pmatrix}\begin{pmatrix}l_2&l_1&l\\-m&m&0\end{pmatrix}\ ,$$

$$C_n^+ = \eta_{\kappa_n}[(l_n+\eta_{\kappa_n}m_n+\tfrac{1}{2})/(2l_n+1)]^{1/2}\ ,$$

$$(n=1,\ 2,\ 1',\ 2')$$

$$C_n^- = [(l_n-\eta_{\kappa_n}m_n+\tfrac{1}{2})/(2l_n+1)]^{1/2}\ ,$$

$$\eta_{\kappa_{1'}}\equiv -\eta_{\kappa_1},\quad \eta_{\kappa_{2'}}\equiv -\eta_{\kappa_2},\quad l_{n'}\equiv l_n',\quad m_{n'}\equiv m_n\ .$$
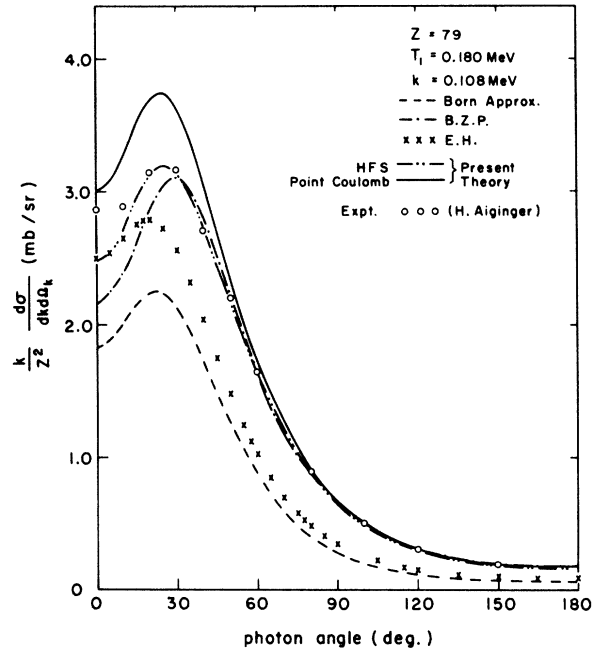
FIG. 12. Comparisons of our results of $\sigma(k,\theta)$ (solid line for point-Coulomb field, double-dotted-broken line for HFS field) with the Born-approximation results (broken line), the results of EH (crosses), the results of BZP (dotted-broken line), and the experimental data of Aiginger (circles) for the case $Z=79$, $T_1=0.180$ MeV, $k=0.108$ MeV.
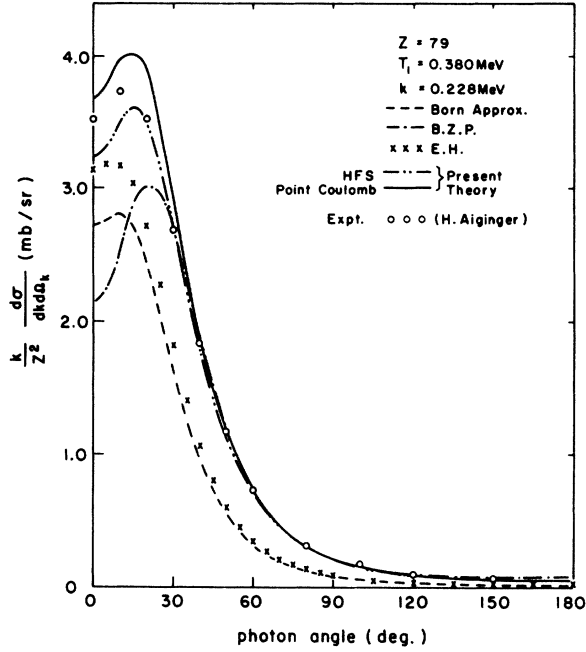
FIG. 13. Comparisons of our results of $\sigma(k, \theta)$ (solid line for point-Coulomb field, double-dotted-broken line for HFS field) with the Born-approximation results (broken line), the results of EH (crosses), the results of BZP (dotted-broken line), and the experimental data of Aiginger (circles) for the case $Z = 79$, $T_1 = 0.380$ MeV, $k = 0.228$ MeV.

Finally, we find

$$S_1 = \int_0^\infty dr \, j_l \,(kr) \, g_{\kappa_1} f_{\kappa_2} \,,$$

$$S_2 = \int_0^\infty dr \, j_l \,(kr) \, g_{\kappa_2} f_{\kappa_1} \,. \qquad (2.10)$$

These s integrals are the basic integrals to be obtained numerically, which will be discussed in Sec. III.

To obtain the unpolarized bremsstrahlung differential cross section we average (2.5) over the initial-electron spin and sum over the final-electron spin and both directions of the polarization of the photon. Upon inserting (2.8) into the expression for $(d\sigma)_{\text{unpol}}$, and integrating over $d\Omega_2$, we obtain[17]

$$\frac{k}{Z^2} \frac{d\sigma}{dk d\Omega_k} \equiv \sigma(k,\,\theta)$$

$$= \lambda_0 \sum_{\kappa_1 \kappa_1 \kappa_2} (-)^{l_1 + \bar{l}_1} \cos(\delta_{\kappa_1} - \delta_{\bar{\kappa}_1}) \sum_{m \equiv |m_2|} [\, A_+^*(m) \bar{A}_+^*(m)$$

$$+ A_+^-(m) \bar{A}_+^-(m) + A_+^*(m) \bar{A}_+^*(m) + A_-^-(m) \bar{A}_-^-(m)]$$

$$\text{(in mb/sr)} \,, \qquad (2.11)$$

where

$$\lambda_0 = [(3.861\,44)^2 \times 10^5] \,(32\alpha/Z^2 p_1) \, E_1 E_2 p_2 k^2 \,,$$

$$A_\pm^*(m) = C_{\kappa_1, m-1}^\pm \, Y_{l_1, m-1 \mp 1/2} \,(\hat{p}_1) R_{\kappa_2 \kappa_1}^+ (m) \,,$$

$$A_\pm^-(m) = C_{\kappa_1, m+1}^\pm \, Y_{l_1, m+1 \mp 1/2} (\hat{p}_1) R_{\kappa_2 \kappa_1}^- (m) \,,$$

the bar over $A_\pm^*$ corresponds to $\bar{\kappa}_1$;

$$R_{\kappa_2 \kappa_1}^\pm (m) = \sum_{n=1}^{2} Q_n^\pm (m) \sum_l {}' P_n^\pm (m) \, s_n \,;$$

and $C_{\kappa, m} \equiv C(l \tfrac{1}{2} j \,; m - s, \, s)$ the Clebsch-Gordan coefficient. Integrating $(d\sigma)_{\text{unpol}}$ over $d\Omega_2$ and $d\Omega_k$, we obtain the unpolarized bremsstrahlung cross section, differential in photon energy:

$$\frac{k}{Z^2} \frac{d\sigma}{dk} \equiv \sigma(k)$$

$$= \lambda_0 \sum_{\kappa_2, \kappa_1, m \equiv |m_2|} \{[R_{\kappa_2 \kappa_1}^+ (m)]^2 + [R_{\kappa_2 \kappa_1}^- (m)]^2\}$$

$$\text{(in mb)}. \qquad (2.12)$$

III. NUMERICAL METHODS

The problem of calculating bremsstrahlung cross sections has been reduced to computing the Q and P factors, the S integrals, and the spherical harmonics. The Q and P factors and the spherical harmonics present no great problem. But the S
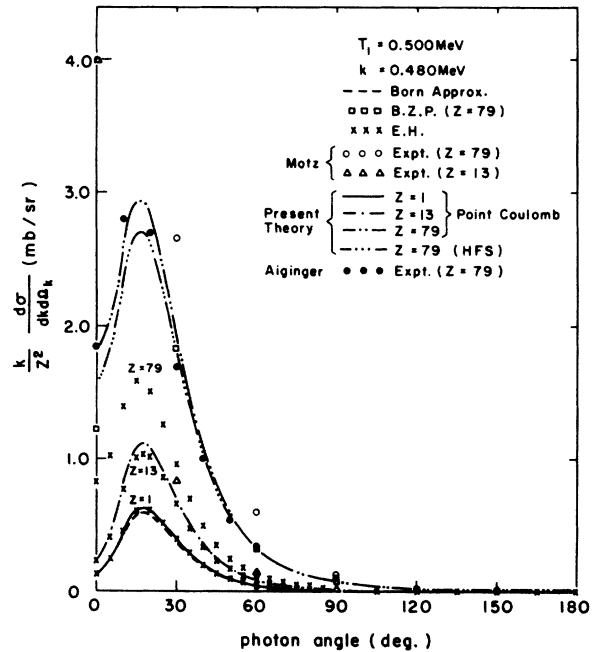
FIG. 14. Comparisons of our results of $\sigma(k, \theta)$ (solid line for $Z = 1$ point-Coulomb field, single-dotted-broken line for $Z = 13$ point-Coulomb field, double-dotted-broken line for $Z = 79$ point-Coulomb field, and triple-dotted-broken line for $Z = 79$ HFS field) with the Born-approximation results (broken line), the results of EH (crosses), the results of BZP (squares for $Z = 79$), and the experimental data of Motz (triangles for $Z = 13$, circles for $Z = 79$) and of Aiginger (solid circles for $Z = 79$) for the cases $T_1 = 0.500$ MeV, $k = 0.480$ MeV, $Z = 1$, 13, and 79.
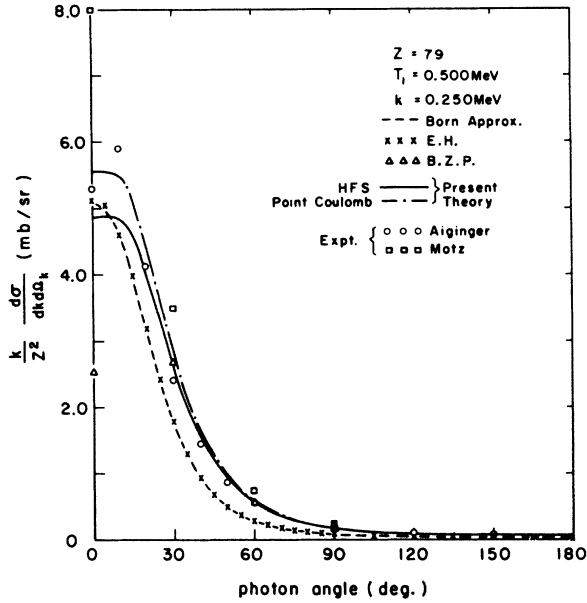
FIG. 15. Bremsstrahlung differential cross sections
$\sigma(k, \theta)$ of present results (solid line for HFS field,
dotted-broken line for point-Coulomb field) for $Z=79$,
$T_1=0.500$ MeV, $k=0.250$ MeV, compared with the Born-
approximation results (broken line), the results of EH
(crosses), the results of BZP (triangles), and the experi-
mental data of Motz (squares) and of Aiginger (circles).
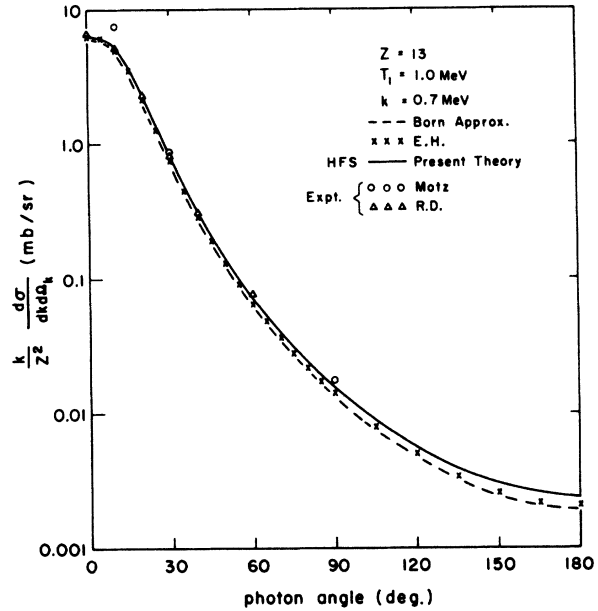
FIG. 16. Bremsstrahlung differential cross sections
$\sigma(k, \theta)$ of present theory (solid line for HFS field) for the
case $Z=13$, $T_1=1.0$ MeV, $k=0.7$ MeV, compared with
the Born-approximation results (broken line), the results
of EH (crosses) and the experimental data of Motz
(circles) and of Rester and Dance (triangles).

integrals must be obtained by numerical integration
of the threefold product of initial continuum wave
functions, final continuum wave functions, and
spherical Bessel functions. Spherical Bessel func-
tions were obtained with the method of Corbató
and Uretsky.[18] The continuum radial wave functions
were obtained by numerical integration of Eq.
(2.7).

In this work we have made calculations for four
different central potentials:

(i) point-Coulomb

$$V(r) = -(Z\alpha/r) \; ; \tag{3.1a}$$

(ii) Thomas-Fermi

$$V(r) = -(Z\alpha/r) \, \tilde{V}_0(a_0 r) \, , \tag{3.1b}$$

$\tilde{V}_0$ is the Thomas-Fermi universal function. Values

of $\tilde{V}_0$ were taken from data of Kobayashi et al.[19];

(iii) modified Thomas-Fermi[20]

$$V(r) = -(Z\alpha/r)(0.711 \, e^{-0.175 a_0 r} + 0.2889 \, e^{-1.6625 a_0 r})^2 \, , \tag{3.1c}$$

with

$$a_0 = 2(\tfrac{3}{4}\pi)^{-2/3} \alpha Z^{1/3} \; ;$$

(iv) modified Hartree-Fock-Slater[21]

$$rV(r) = -Z + \int_0^r n(r') \, dr' + r \int_r^\infty [n(r')/r'] \, dr'$$

$$-\tfrac{2}{3} [(81/32\pi^2) \, r \, n(r)]^{1/3} \, , \tag{3.1d}$$

with $n(r) = 4\pi r^2 \rho(r)$ the radial electron charge den-
sity. The radial charge density used in this work
was obtained from Liberman.[21]

The continuum wave functions were computed with
similar methods to those used by Schmickley and

TABLE II. Comparison of point-Coulomb Bremsstrahlung cross sections $\sigma(k)$ as calculated by the Born approxima-
tion, BZP or ZB, EH, and the present authors for $Z=1$ cases.

					Born	BZP or ZB	EH	Present theory
	0.380		0.228		4.477	4.425	4.513	4.513
$\sigma(k)$ (mb) for $T_1 =$		Mev, $k =$		Mev				
	0.500		0.250		4.984	4.29	5.003	4.985

TABLE III. Comparison of point-Coulomb Brems-strahlung cross sections $\sigma(k)$ in millibarns as calculated from nonrelativistic theory with retardation (N. R. W. R.), Sommerfeld theory without retardation (N. R. W. O. R.), and the present work for low-energy cases.

Z	T_1 (Mev)	k (Mev)	β_1 N.R.	β_2 N.R.	N.R.W.O.R.	N.R.W.R.	This work (Point-Coulomb)
13	0.005	0.004	0.14	0.063	332.	344.	335.
13	0.045	0.040	0.42	0.14	28.1	41.2	28.0
13	0.050	0.020	0.44	0.34	37.6	60.4	40.3
79	0.050	0.020	0.44	0.34	38.1	53.0	46.7

Pratt. [8] In order to have a finite solution at the origin we convert g and f in Eq. (2.7) to $\bar{g}$ and $\bar{f}$, respectively, where $\bar{g} = r^{-\gamma}g$, $\bar{f} = r^{-\gamma}f$, $\gamma = [\kappa^2 - (Z\alpha)^2]^{1/2}$. To reduce the propagation error, we use the power-series-expansion method to compute the first $2(1 + I_0)$ points, where I_0 is defined by $|\kappa| = 2I_0 + I_R$, with $0 \le I_R < 2$. The integration was continued by the fourth-order Runge-Kutta method. [22] Upon reaching the first minimum of $\bar{f}$, near $r = |\kappa|/p$, we switched from computing $\bar{g}$ and $\bar{f}$ to computing g and f. It is desirable to do this because these functions are asymptotically sinusoidal.

The functions g and f are normalized by a spherical-Bessel-function formulation based on the assumption that at some point in the free-field region of the atom the wave functions g and f are approximately modified phase-shifted free-field solutions:

$$g = r[(E+1)/2E]^{1/2}[A_+ j_\kappa(pr) - A_- y_\kappa(pr)],$$

$$f = r[(E-1)/2E]^{1/2}[A_+ j_{\kappa-1}(pr) - A_- y_{\kappa-1}(pr)];$$

or

$$g = r[(E+1)/2E]^{1/2} A[\cos\bar{\delta}_\kappa j_\kappa(pr) - \sin\bar{\delta}_\kappa y_\kappa(pr)],$$

$$f = r[(E-1)/2E]^{1/2} A[\cos\bar{\delta}_\kappa j_{\kappa-1}(pr) - \sin\bar{\delta}_\kappa y_{\kappa-1}(pr)],$$

where

$$\bar{\delta}_\kappa \equiv \tilde{\delta}_\kappa + Q, \quad A = (A_+^2 + A_-^2)^{1/2},$$

$$\tilde{\delta}_\kappa \equiv \delta_\kappa - (l - \kappa)\tfrac{1}{2}\pi,$$

$$\bar{\delta}_\kappa = \tan^{-1}(A_-/A_+) \quad \text{if} \quad A_+ > 0; \qquad (3.2)$$

$$\bar{\delta}_\kappa = \tan^{-1}(A_-/A_+) + \pi \quad \text{if} \quad A_+ < 0, \ A_- > 0;$$

$$\bar{\delta}_\kappa = \tan^{-1}(A_-/A_+) - \pi \quad \text{if} \quad A_+ < 0, \ A_- < 0.$$

Q, the phase correction integral, is defined by

$$\frac{dQ}{dr} \equiv \frac{\nu \tilde{V}}{r},$$

where

$$\nu = \frac{Z\alpha E}{p}, \quad \tilde{V} = \frac{V}{-Z\alpha/r}$$

$Q = \nu \ln 2pr$ for point-Coulomb field,

$$\qquad (3.3)$$

$$= (E/p) \int_r^\infty V(w)dw \quad \text{for screened fields}.$$

In order to have the following normalized solutions:

$$g = r[(E+1)/2E]^{1/2}[\cos\bar{\delta}_\kappa j_\kappa(pr) - \sin\bar{\delta}_\kappa y_\kappa(pr)],$$

$$\qquad (3.4)$$

$$f = r[(E-1)/2E]^{1/2}[\cos\bar{\delta}_\kappa j_{\kappa-1}(pr) - \sin\bar{\delta}_\kappa y_{\kappa-1}(pr)],$$

the normalized solutions should be multiplied by the normalization constant $N = A^{-1}$. By averaging A and $\bar{\delta}_\kappa$ over one (or more) period(s), we get better results for normalizations and phases.

Combining the normalized initial and final radial wave functions with the spherical Bessel functions, we numerically integrated the S integrals by the tenth-order Newton-Cotes formula, with the integration grid $\Delta r = \pi/(32p_1)$ up to the point where the continuum wave functions can be approximately considered as the modified phase-shifted free-field wave functions and an integration-by-parts method can be used. Then the rest of the S integrals were calculated by
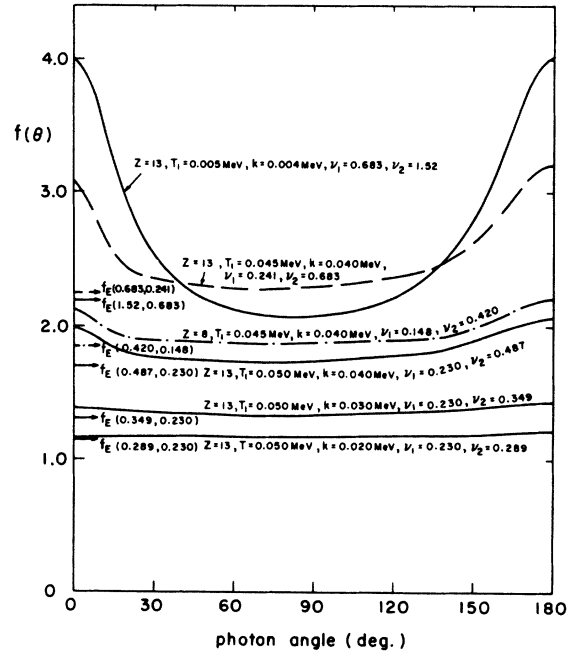
FIG. 17. Coulomb correction factors $f(\theta)$ for the cases (1) $Z = 13$, $T_1 = 0.005$ MeV, $k = 0.004$ MeV; (2) $Z = 13$, $T_1 = 0.045$ MeV, $k = 0.040$ MeV; (3) $Z = 8$, $T_1 = 0.045$ MeV, $k = 0.040$ MeV; (4) $Z = 13$, $T_1 = 0.050$ MeV, $k = 0.040$ MeV; (5) $Z = 13$, $T_1 = 0.050$ MeV, $k = 0.030$ MeV; (6) $Z = 13$, $T_1 = 0.050$ MeV, $k = 0.020$ MeV. Elwert factors $f_E(\nu_2, \nu_1)$ are shown by arrows.
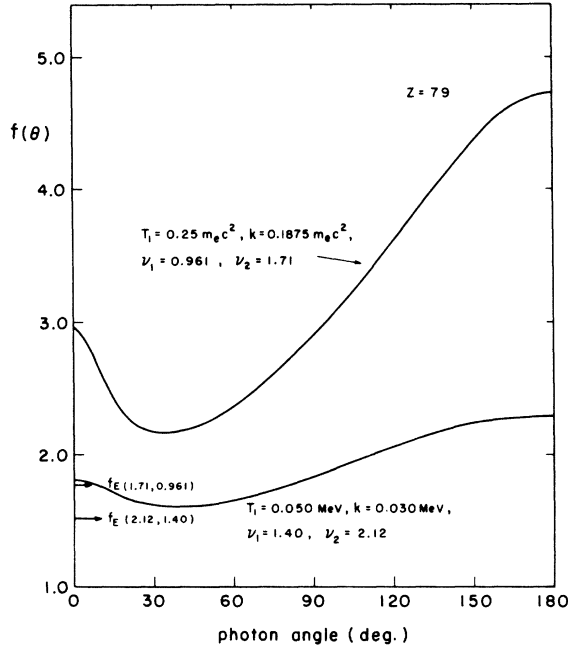
FIG. 18. Coulomb correction factors $f(\theta)$ for the cases $Z=79$, $T_1=0.25\ m_e c^2$, $k=0.1875\ m_e c^2$, and $Z=79$, $T_1 =0.050$ MeV, $k=0.030$ MeV. Elwert factors $f_E(\nu_2, \nu_1)$ are shown by arrows.

the integration-by-parts method.[4] The S integrals were combined with the Q and P factors to give R matrices, and these were combined to give the cross section, differential in photon energy. Combining the R matrices with the Clebsch-Gordan coefficients and the spherical harmonics we obtain the cross section, differential in photon energy and angle.

We should finally discuss the accuracy of our numerical methods. Errors in the calculations of wave functions are discussed in the paper of Pratt et al.,[23] and present errors are of the same order, $\lesssim 10^{-4}$. Errors in spherical Bessel functions, spherical harmonics, 3-j symbols, etc., are completely negligible. The two major sources of error are (i) finite grid size in the S integration (histogram error), and (ii) truncation error due to limitation of the number of κ_1's and of κ_2's in the series Eqs. (2.11) and (2.12).

To estimate the histogram errors in S integrals we made tests by using various grid sizes ranging $\pi/(128p_1)-\pi/(16p_1)$. The results generally fluctuated by $O(0.1\%)^{24}$ for $\sigma(k)$, $O(1\%)$ for $\sigma(k, \theta)$ with small and large photon angles, $O(0.1\%)$ for intermediate photon angles. The other major source of error, truncation, can be tested by increasing the number of κ_1's and of κ_2's. The results show the same order of fluctuations as those by the histogram errors. The number of κ_1's and of κ_2's used in this work is

given in Table I.

The combined effects of all errors are estimated to be $O(1\%)$ for $\sigma(k, \theta)$, and $O(0.5\%)$ for $\sigma(k)$ results.

IV. RESULTS AND DISCUSSION

We list in Table I all cases (specified by Z, T_1, and k) we have computed. The Table also gives the bremsstrahlung cross section $\sigma(k)$ integrated over angles which we obtained with different potential models; these values correspond to single points in the energy spectrum of the bremsstrahlung. In Figs. 2–16 we show the corresponding angular distributions $\sigma(k, \theta)$ in millibarns per steradian for each of these cases, as well as a comparison with other work. Our cases provide some coverage of the energy range 5 KeV–1 MeV and targets $Z = 1 - 79$; they were chosen to study Coulomb corrections and screening effects and to permit comparisons with previous work. We begin by comparing point-Coulomb potential results which also serve as a check of our calculations. We can then discuss the importance of Coulomb effects beyond the Born approximation (Bethe-Heitler formula). Next we examine the importance of screening effects. After summarizing our theoretical formulation we compare it with current experimental work.

A. Comparison of Point-Coulomb Results

We compare the point-Coulomb-potential results
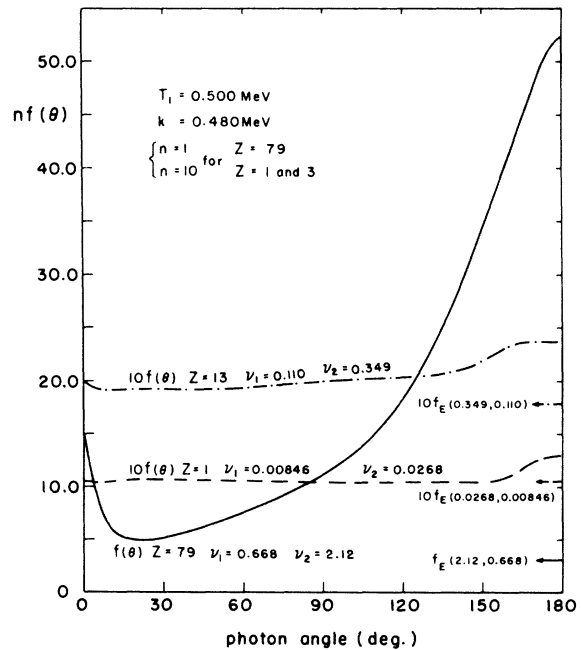
FIG. 19. Coulomb correction factors $f(\theta)$ for the cases $T_1=0.500$ MeV, $k=0.480$ MeV, $Z=1$, 13, and 79. Elwert factors $f_E(\nu_2, \nu_1)$ are shown by arrows.

H. K. TSENG AND R. H. PRATT

TABLE IV. Comparison of Coulomb correction factors $f(v_2, v_1)$ calculated in the present work with the Elwert factors f_E for all the cases given in Table I, and comparison of the screening correction factors $\gamma(k)$ calculated with the Born-approximation theory and in the present work.

Z	T_1 (MeV)	k (MeV)	$f(v_2, v_1)$	f_E	$\gamma^B(k)$ HFS	$\gamma^B(k)$ TFC	$\gamma^{cal}(k)$ HFS	$\gamma^{cal}(k)$ TFC	$\gamma^{cal}(k)$ TF	$v_2 - v_1$	ξ_s
1	0.500	0.480	1.063	1.058	•••	•••	•••	•••	•••	0.02	67.
1	0.500	0.250	1.000	1.004	•••	•••	•••	•••	•••	0.001	16.
1	0.380	0.228	1.008	1.008	•••	•••	•••	•••	•••	0.002	21.
8	0.045	0.040	1.883	1.851	•••	•••	•••	•••	•••	0.27	14.
13	0.005	0.004	2.206	2.193	0.862	0.893	0.882	0.860	0.845	0.84	4.1
13	0.045	0.040	2.317	2.243	0.985	•••	0.986	•••	•••	0.44	12.
13	0.050	0.040	1.752	1.697	0.982	0.985	0.982	0.972	•••	0.26	10.
13	0.050	0.030	1.342	1.306	0.967	0.976	0.975	0.965	•••	0.12	6.5
13	0.050	0.020	1.171	1.147	0.941	•••	0.960	•••	•••	0.06	3.9
13	0.500	0.480	1.903	1.782	•••	•••	•••	•••	•••	0.24	28.
13	1.000	0.700	1.120	1.061	0.996	•••	0.997	•••	•••	0.01	11.
79	0.050	0.030	1.755	1.518	0.899	0.931	0.836	0.848	•••	0.72	3.6
79	0.050	0.020	1.356	1.257	0.857	•••	0.798	•••	•••	0.36	2.1
79	$0.25\, m_e c^2$	$0.1875\, m_e c^2$	2.488	1.771	0.948	•••	0.904	•••	•••	0.75	6.5
79	0.180	0.108	1.943	1.393	0.944	•••	0.910	•••	•••	0.34	4.8
79	0.380	0.228	1.904	1.275	0.955	•••	0.932	•••	•••	0.20	5.0
79	0.500	0.480	5.954	3.126	0.978	•••	0.945	•••	•••	1.45	16.
79	0.500	0.250	1.634	1.156	0.947	•••	0.921	•••	•••	0.11	3.7

with analytic theoretical predictions in two limiting cases: (a) for very small Z, with the Born approximation[1] and (b) for very low energy, with nonrelativistic results.[3]

Relativistic Born approximation (the Bethe-Heitler formula) is expected to be valid when the Coulomb parameter $\gamma_B \equiv 2\pi Z \alpha/\beta_2 \ll 1$. Values of γ_B for our cases are shown in Table I. The $Z = 1$ cases shown in Table II were run specifically to check our calculations; in Table II we compare them with other results. The integrated results are within 1% of the Born approximation and are higher; it will be clear from our subsequent comparison with the Elwert-Haug calculations[25] that this is a real deviation from the Born approximation. In angular distributions this deviation arises from intermediate photon angles, as in Figs. 2 and 3. However, we believe the deviations these figures also show at small and large angles, which do not contribute in the integrated result, are not real: More partial waves are required at these angles. (We saw this greater sensitivity both in our own work and in the various forms of the BZP results.[5,26] We estimate that to obtain about 2% accuracy at these angles would require about twice the number of partial waves used in this work.) It may be noted that throughout the low-energy region the Born approximation underestimates the cross section. Much of the underestimate is simply a normalization factor and we will discuss this later. We know, however, from the work of Bethe and Maximon, that a crossover takes place, and at high energies Born approximation is an overestimate. Thus for lead and en-

ergies above 50 MeV the Bethe-Heitler formula tends to overestimate cross sections by about 10%.[2]

Nonrelativistic results may be expected to be valid when the initial electron kinetic energy $T_1 \ll 1$ and the screening is small. The condition $T_1 \ll 1$ is most nearly achieved in the cases shown in Figs. 4–10, and particularly in the case $Z = 13$, $T_1 = 5$ keV, $k = 4$ keV (Fig. 4). The standard result (no retardation) obtained by Sommerfeld is only valid when β_1 is small compared to unity. However, the theory neglects screening effects, which are important for very low energies, and we will discuss this later. It is also possible to include certain retardation effects, as originally done by Elwert[6] and more recently by Elwert and Haug,[6] as a limit of their relativistic calculation, namely, by neglecting $O(\beta^2)$ in their formula. There are problems of consistency because $O(\beta)$ terms are also partly neglected, as in $(e^{2\pi a/\beta} - 1)$, since $\beta = \beta_{NR}[1 + O(\beta^2)]$, where NR stands for nonrelativistic kinematics. In Figs. 4, 5, 8, and 10 we have shown both treatments,[27] and the corresponding integrated results are summarized in Table III, which also gives the β_{NR}. We see that for 5 keV, by including retardation effects, we get agreement for the integrated cross section within 3%, as well as a good fit of the angular distribution. Thus, even at our lowest energy we have seen that retardation effects are important, but in fact the relativistic Born approximation includes them. At higher energies the β are already too large to expect more than qualitative agreement. The retardation continues to improve the shape, but the integrated values actually run
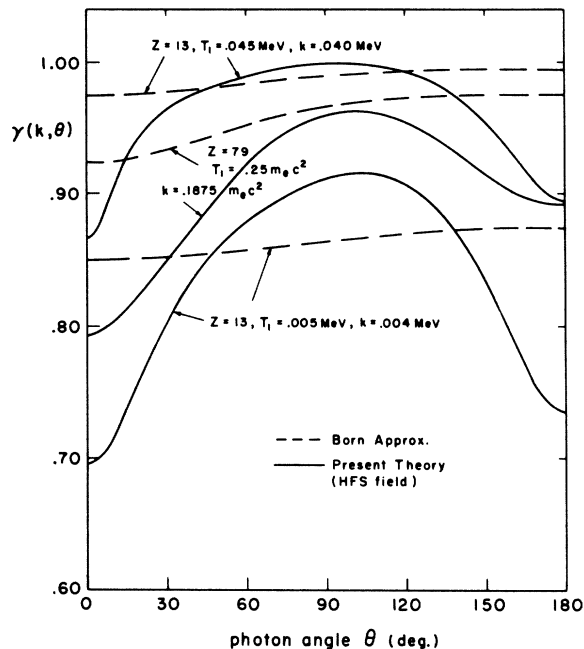
FIG. 20. Screening correction factors $\gamma(k, \theta)$ for the cases $Z = 13$, $T_1 = 0.005$ MeV, $k = 0.004$ MeV, $Z = 13$, $T_1 = 0.045$ MeV, $k = 0.040$ MeV, and $Z = 79$, $T_1 = 0.25$ $m_e c^2$, $k = 0.1875$ $m_e c^2$.

closer to the calculation without retardation.

We can also compare the point-Coulomb-potential case with the recent analytic work of Elwert and Haug (EH). This calculation uses Sommerfeld-Maue (SM) wave functions,[28] neglecting screening effects, and in appropriate limits reduces to the formulas of Sommerfeld,[3] Elwert,[3] Bethe and Heitler,[1] Sauter,[1] Scherzer,[29] and Bethe and Maximon.[2] The SM wave function is a good approximation for all energies provided $(Z\alpha)^2/|\kappa| \ll 1$ and the screening is small. For $Z = 1$, 8, and 13 our results are quite close to Elwert-Haug predictions at all energies, although the deviations are significant and indicate that the Elwert-Haug formula underestimates the Coulomb cross sections $\sigma(k)$ and $\sigma(k, \theta)$. The agreement is better for lower-Z cases, and disappears in the high-Z cases. This shows the growing importance of the higher-order terms in Z which the EH calculation neglects. For high Z, the EH results appear little different from the Born-approximation results when the outgoing electron carries a substantial fraction of the energy, but are better (though not good) for the cases in which the Born-approximation results are worst, namely, for much of the energy radiated. One understands this when one remembers that in the extreme case of the tip (all energy radiated), the Born-approximation result vanishes, but because the nuclear field strongly distorts the low-energy wave function from that of a plane wave, the cross section in fact

remains finite.[3,30] The SM wave function includes this distortion and so the EH formula correctly gives finite results. This feature is also related to the Elwert factor,[6] as will be discussed shortly.

Two previous attempts at numerical calculation can be compared with our point-Coulomb results. One case was obtained by Rozics and Johnson (RJ),[31] using exact electron-point-Coulomb wave functions in a partial-wave expansion. Comparison of our point-Coulomb results with those of RJ is given in Fig. 11. The disagreement is probably due to the fact that the RJ calculation does not include enough partial-wave terms. This difficulty is more clearly visible in the work of BZP, which we see in three stages with increasing numbers of partial waves taken. The earliest form,[26] shown in Fig. 3, improved in the published results[5] of Figs. 2 and 12–15. Subsequent work was done by Rester and Peasley,[32] who have had access to the BZP codes. The agreement with the Born approximation and EH for the $Z = 1$ cases shown in Table II gives us greater confidence in our results, but we conclude that the BZP results are acceptable for integrated cross sections $\sigma(k)$, though not for the angular distribution $\sigma(k, \theta)$.

B. Coulomb Effects

In order to formulate in more detail the Coulomb effects that go beyond the Bethe-Heitler formula, we have plotted the ratio $f(\theta) \equiv \sigma^{\text{Coul}}(k, \theta)/\sigma^{\text{Born}}(k, \theta)$
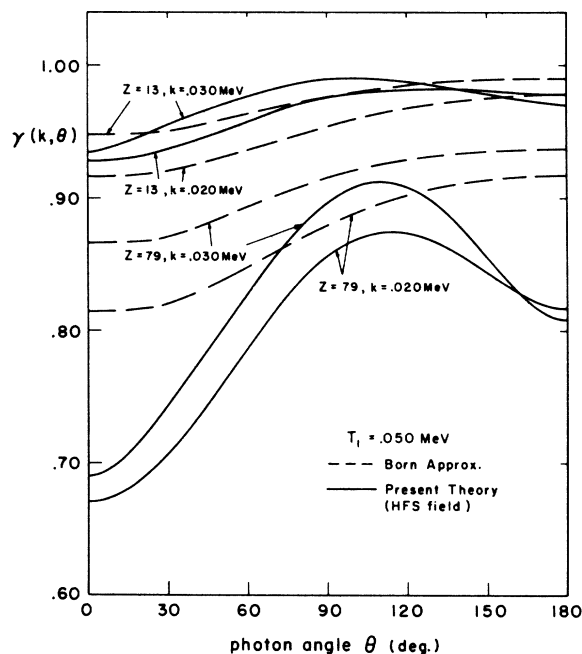
FIG. 21. Screening correction factors $\gamma(k, \theta)$ for the cases $T_1 = 0.050$ MeV, $k = 0.030$ MeV, and 0.020 MeV, $Z = 13$ and 79.

of point-Coulomb to Bethe-Heitler angular distribu-
tion in some representative cases in Figs. 17–19.
Table IV gives the integrated Coulomb-correction
factor $f(\nu_2,\ \nu_1) = \sigma^{Coul}(k)/\sigma^{Born}(k)$. In almost all
the cases we have considered, even for $Z = 13$,
Coulomb effects are very large. However, we be-
lieve that such effects are fairly small for low Z
when less than half the energy is radiated.

It is apparent that in many cases the shape of the
angular distribution is given well by the Born-ap-
proximation theory, and the Coulomb effect is
presumably a normalization effect.

Such a prediction was obtained by Elwert in the
nonrelativistic region, by comparing the nonrelativ-
istic Born approximation and the exact nonrelativ-
istic calculation without retardation, giving (Elwert
factor)[6]

$$f_E(\nu_2,\ \nu_1) = (\nu_2/\nu_1)(1 - e^{-2\pi\nu_1})/(1 - e^{-2\pi\nu_2}) \qquad (4.1)$$

independent of the angle. This derivation requires
$T_1 \ll 1$ and $(\nu_2 - \nu_1) \ll 1$. The factors arise from the
normalization of continuum Coulomb wave functions –
in the low-energy limit they keep these wave func-
tions finite. We have plotted f_E for all the angular
distributions in Figs. 17–19, and we give its val-
ues for all our cases in Table IV. It is clear that
the usefulness of the idea of normalization goes be-
yond the regions for which Elwert's derivation ap-
plies. Note that f_E approaches 1 as the energy ra-
diated becomes small.

From the figures we can see that higher Born-
approximation corrections (Coulomb effects) that
go beyond simple normalization are important for
small and for large photon angles. In the present
energy range they increase the cross section. This
has consequences for screening which we will dis-
cuss below. Such effects grow with increasing
atomic number Z and also as the ratio k/T_1 in-
creases. Since small and large angles contribute
less to integrated cross sections, it appears pos-
sible, according to Table IV, to use the factor f_E
to predict such cross sections for low-Z elements
and initial electron kinetic energies below about
0.1 MeV (or with 10% accuracy up to 1 MeV).
However, for high-Z elements, the Elwert factor
gives poor predictions even at low energies. This
conclusion was also reached by Elwert and Haug.
There are not yet enough data to construct with con-
fidence an empirical $f(\nu_2,\ \nu_1)$ valid over wider
ranges.

C. Screening effects

We now turn to a discussion of the effects of elec-
tron screening on the point-Coulomb cross sections
we have considered to understand when screening
effects are important and to see whether they can
be estimated in any simple fashion. Until now,
such estimates have been made with a form-factor

approach based on the Born approximation; so we
will examine in some detail the validity of this pro-
cedure.

We have considered primarily the modified Har-
tree-Fock-Slater potential, but we also have a few
results for TFC and TF potential models which en-
able us to see the sensitivity to the choice of screen-
ing-potential model. Ratios of screened to Cou-
lomb distributions are presented for some of our
cases in Figs. 20–22, and ratios of the integrated
results are given in Table IV. Differences between
screening models at these energies are about 1%
and so we will not discuss them further – this
stability assures us of the physical validity of our
results. (It does appear that sensitivity to the
screening models increases at very low energies.)

We compare our results with those of BZP, the
only other calculation which goes beyond form-fac-
tor approximation, in Figs. 6–10 and 12–15. The
agreement is fairly good, particularly in the (un-
published) BZRP cases, for which their codes were
further modified. We have already noted in dis-
cussing the point-Coulomb cases that the BZP re-
sults are not good at small and large photon angles;
we find BZRP an improvement although some dif-
ferences still remain, especially for smaller k/T_1
ratio cases. For the screened integrated cross
sections no BZP results were published, but they
can be obtained by integrating the BZP results over
the photon angle.
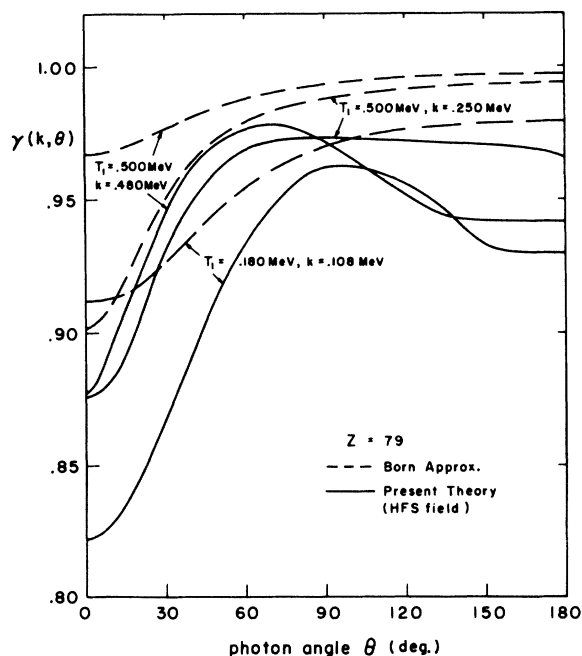
FIG. 22. Screening correction factors $\gamma(k, \theta)$ for the
cases $Z = 79$, $T_1 = 0.500$ MeV, $k = 0.250$ MeV, and 0.480
MeV; and $Z = 79$, $T_1 = 0.180$ MeV, $k = 0.108$ MeV.

Let us now review the usual theory of screening and the regions in which it is claimed to be valid. In the Born approximation, the bremsstrahlung matrix element is proportional to

$$\int V(r)\, e^{i\vec{q}\cdot\vec{r}}\, d^3r \equiv M' \;,$$

where

$$V(r) = \int [\rho_N(r') + \rho_e(r')]\, d^3r' / |\vec{r} - \vec{r}'| \;, \qquad (4.2)$$

ρ_N and ρ_e are the nuclear-charge and electron-charge densities, respectively; $\vec{q} = \vec{p}_1 - \vec{p}_2 - \vec{k}$ is the momentum transferred to the nucleus.[33] From Eq. (4.2) we have

$$M' = (4\pi Z/q^2)[F_N(q) + F_e(q)] \;,$$

with

$$F_N(q) = (1/Z)\int \rho_N(r)\, e^{i\vec{q}\cdot\vec{r}}\, d^3r \;,$$
$$F_e(q) = (1/Z)\int \rho_e(r)\, e^{i\vec{q}\cdot\vec{r}}\, d^3r \;. \qquad (4.3)$$

In the energy region considered in this paper we have $F_N(q) \cong 1$.[34] Thus the unscreened cross section may be corrected for screening effects by including the multiplication factor $[1 - F_e(q)]^2$. If the analytic form of the potential model is known, the form factor can be calculated by the method developed by Molière.[35] For our comparisons, the electron form factors $F_e(q)$ were computed numerically using the Hartree-Fock-Slater (HFS) radial-electron charge density.

The standard description of screening effects in bremsstrahlung[36,37] is based on the parameters of the Thomas-Fermi model. Here $F_e(q)$ depends on the quantity qr_{TF}, where $r_{TF} = 137\, Z^{-1/3}$ is the radius of the Thomas-Fermi atom. Screening effects are classified by the screening parameter ξ_s which is

approximately equal to r_{TF}/r_{max}, where r_{max} is the maximum-impact parameter discussed by Heitler[36] and is equal to q_{min}^{-1}, $q_{min} = p_1 - p_2 - k$. If r_{max} is small compared to r_{TF}, then ξ_s is large and $F_e(q)$ is small, which means electron screening is not important. If r_{max} is of the order of r_{TF}, then $\xi_s \sim 1$, F_e is large, and screening is important. A comparison of r_{max} with r_{TF} in the energy range we considered here is shown in Fig. 23. One sees that screening effects are important for high and low energies. For a given incident energy the effects are more important when less energy is radiated.

In Table IV we show our results for the ratio $\gamma^{cal}(k)$ of screened to point-Coulomb-integrated cross sections and compare them with $\gamma^B(k)$ as calculated from the form-factor theory. This Table also gives the parameter ξ_s which indicates the expected importance of screening. The calculated screening correction factor $\gamma^{cal}(k)$ for the HFS field is also plotted in Fig. 23, allowing one to see the regions for which screening in fact is important. Then in Figs. 20-22 we show the corresponding ratios $\gamma(k, \theta)$ for angular distributions in some representative cases. From Table IV and Fig. 23 we see that the criterion for importance of screening based on ξ_s is qualitatively correct, but the screening effects tend to be larger than usually supposed. For the same parameter ξ_s the screening is more important for large Z and for small or large T_1, i.e., the ranges in which screening is unimportant are more limited than the form-factor theory suggests. It may be noted that, in general, the cases for which screening corrections are expected to be large are those which are difficult to calculate with our techniques because such a large number of partial waves are required. These are cases in which
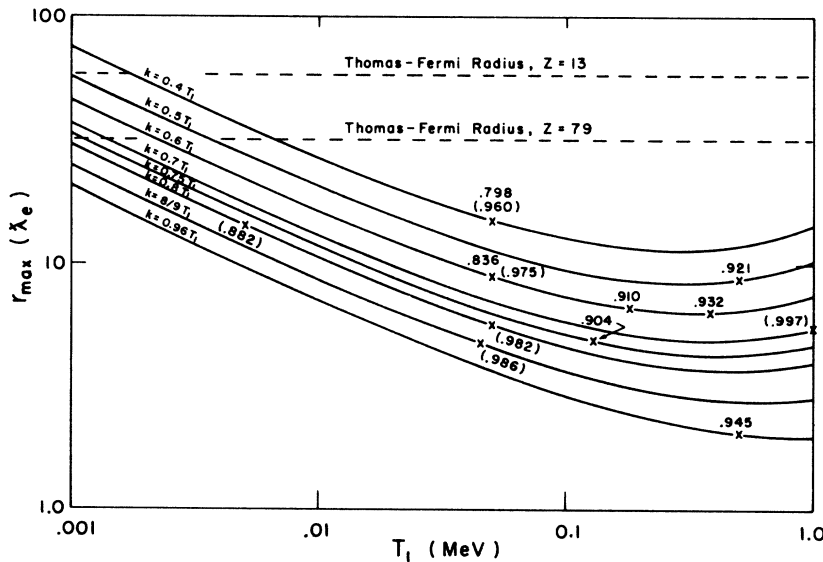
FIG. 23. Comparison of the maximum impact parameter r_{max} with the radius of the Thomas-Fermi atom r_{TF} in the energy range $T_1 = 0.001-1.0$ MeV. (λ_e in the figure is the compton wavelength.) The calculated screening correction factors $\gamma^{cal}(k)$ for the HFS field are superimposed on the figure for all our $Z = 13$ and 79 cases; the numbers given in the parentheses are for the $Z = 13$ cases. The cases are indicated with X's.

higher Born effects are important, small- or large-angle regions are important; in such regions more partial waves are required.

In the range we have calculated, with the screening factor $\gamma(k)$ generally greater than 0. 9 for low-atomic-number elements, γ^B gives at least a qualitative impression of screening and often gives the cross section within 2%. However, for those cases in which screening effects are big, the form-factor theory of screening appears to give poor predictions.

Looking at the angular distributions, we see that the form-factor approach is most satisfactory at intermediate angles. We understand this once we remember that this is a Born-approximation result, and we have already seen that, apart from over-all normalization, the Born approximation is good at intermediate angles. At large and small angles, we find that higher Born approximations increase the cross section; when screening is included, form factors should be folded in multiply, which explains why the actual calculated screening factors $\gamma(k, \theta)$ are smaller at small and large angles. Since the intermediate angles dominate the integrated cross section, the deviations there are not so large.

It appears that screening effects, like Coulomb effects, should be described by an empirical γ. Again, there are not yet sufficient data to construct such a γ with confidence.

D. Comparison with Experiments

The status of experimental work on the bremsstrahlung cross section to 1958 has been summarized by Koch and Motz[37] in a review article on this process. For incident-electron kinetic energies of 15–50 keV, results were obtained by Smick and Kirkpatrick, Clark and Kelly, Amrehn, Bohm, Honerjager, Amrehn and Kulenkampff, Kerscher and Kulenkampff, Doffin and Kulenkampff, Röss,[38] and Motz and Placious[39]; 90–180 keV by Mausbeck, and Zeh[40]; 0. 5–1. 0 MeV by Motz[41]; and 2. 72, 4. 54, and 9. 66 MeV by Starfelt and Koch.[42]

Recently, Rester and Dance,[43] and Rester[44] have reported experimental data for electron kinetic energies of 1.0, 1.7, 2.0, and 2.5 MeV. They show disagreement with the results of Motz for Al and Au at 1.0 MeV. For electron kinetic energies of 2.04 MeV, results have been reported recently by Aiginger and Zinke[45]; of 0.180 and 0.380 MeV by Aiginger[46]; of 0.500 MeV by Aiginger[47]; and of 50 and 200 keV by Rester.[48]

Figures 6–10 present comparisons of our HFS results with the experimental data of Motz and Placious (MP)[39] and of Rester[48] for the cases T_1 = 0. 050 MeV; k = 0. 040, 0. 030, and 0. 020 MeV (for Z = 13); k = 0. 030 and 0. 020 MeV (for Z = 79). The experimental data of Rester are closer to our HFS results than those of MP.

In Fig. 16 we give a comparison of our HFS results with the experimental data of Motz[41] and of Rester and Dance (RD)[43] for the case Z = 13, T_1 = 1. 0 MeV, k = 0. 7 MeV. The experimental data of RD are closer to our results than those of Motz, especially for small photon angles.

For the cases Z = 79, T_1 = 0. 180 MeV, k = 0. 108 MeV, and Z = 79, T_1 = 0. 380 MeV, k = 0. 228 MeV as shown in Figs. 12 and 13, we find good agreement with the experimental data of Aiginger.[46]

Finally, in Figs. 14 and 15 we present comparisons of our results with the experimental data of Motz[41] and of Aiginger[47] for the cases T_1 = 0. 5 MeV, k = 0. 480 MeV, and T_1 = 0. 5 MeV, k = 0. 250 MeV. The experimental data of Motz are high and the experimental data of Aiginger agree well with our results.

From these examples, we conclude that the agreement between the experimental results of Aiginger, and of Rester and Dance and our HFS results is quite good. The experimental data of Motz are seen to overestimate the cross section. The recent experimental data of Rester are closer to our HFS results than those of Motz and Placious.

ACKNOWLEDGMENTS

*Supported in part by U. S. Atomic Energy Commission, under Contract No. AT-(30-1)-3829.

[1]H. A. Bethe and W. Heitler, Proc. Roy. Soc. (London) A146, 83 (1934); F. Sauter, Ann. Physik 20, 404 (1934); G. Racah, Nuovo Cimento 11, 461 (1934); 11, 467 (1934).

[2]H. A. Bethe and L. C. Maximon, Phys. Rev. 93, 738 (1954); H. Davies, H. A. Bethe, and L. C. Maximon, ibid. 93, 788 (1954); H. Olsen, L. C. Maximon, and H. Wergeland, ibid. 106, 27 (1957); H. Olsen and L. C. Maximon, ibid. 114, 887 (1957); A. Sørenssen, Nuovo Cimento 38, 745 (1965); 41, 543 (1966).

[3]A. Sommerfeld, Ann. Physik 11, 257 (1931); G. Elwert, ibid. 34, 178 (1939); P. Kirkpatrick and L. Wied-

mann, Phys. Rev. 67, 321 (1945).

[4]More detailed discussion can be found in H. K. Tseng, Ph. D. dissertation, University of Pittsburgh, 1970 (unpublished).

[5]H. Brysk, C. D. Zerby, and S. K. Penny, Phys. Rev. 180, 104 (1969).

[6]G. Elwert and E. Haug, Phys. Rev. 183, 90 (1969).

[7]H. K. Tseng and R. H. Pratt, Phys. Rev. A 1, 528 (1970).

[8]R. D. Schmickley and R. H. Pratt, Phys. Rev. 164, 104 (1967).

[9]H. Bethe, Proc. Cambridge Phil. Soc. 30, 524 (1934); Ann. Physik 5, 385 (1930).

[10]H. W. Furry, Phys. Rev. 81, 115 (1951).

[11]F. J. Dyson, Phys. Rev. 75, 486 (1949); 75, 1736 (1949); R. P. Feynman ibid. 76, 749 (1949); 76, 769 (1949).

[12]P. I. Fomin, Zh. Eksperim. i Teor. Fiz. 35, 707 (1958) [Soviet Phys. JETP 8, 491 (1959)]; K. J. Mork and H. Olsen, Phys. Rev. 140, B1661 (1965); 166, 1862 (1968).

[13]G. Källen, in Handbüch der Physik, Vol. V/1 edited by S. Flügge (Springer, Berlin, 1958), p. 226; G. Källen, Topics in Quantum Electrodynamics, 1962; Brandeis Lecturer, Vol. 1 (Benjamin, New York, 1962), p. 123. We deal with particle densities normalized to 1 per unit volume and use the unrationalized natural unit system, i.e., $\hbar = m_e = c = 1$. We follow the notation of J. D. Bjorken and S. D. Drell, Relativistic Quantum Mechanics (McGraw-Hill, New York, 1964) and Relativistic Quantum Fields (McGraw-Hill, New York, 1965).

[14]N. F. Mott and H. S. W. Massey, Atomic Collisions, 1st ed. (Oxford U. P., London, 1933), p. 82; A. Sommerfeld, Atombau and Spektrallinien, Vol. 2 (F. Vieweg and Son, Braunschweig, 1939), p. 457. H. A. Bethe, L. C. Maximon, and F. Low, Phys. Rev. 91, 417 (1953).

[15]M. E. Rose, Relativistic Electron Theory (Wiley, New York, 1961), p. 207. If we choose $\hat{p}$ along the z axis, then Eq. (2.6) gives Darwin's solutions of the Dirac equation in a closed form and is especially convenient for calculating potential scattering. C. G. Darwin, Proc. Roy. Soc. (London) A 118, 654, (1928).

[16]Here the Condon-Shortley phase convention is chosen.

[17]From now on we drop the subscript unpol and all the results considered in this paper are unpolarized case.

[18]F. J. Corbató and J. L. Uretsky, J. Assoc. Comp. Mach. 6, 366 (1959).

[19]S. Kobayashi, T. Matsukuma, S. Nagai, and K. Umeda, J. Phys. Soc. Japan 10, 759 (1955).

[20]P. Csavinszky, Phys. Rev. 166, 53 (1968).

[21]W. Kohn and L. S. Sham, Phys. Rev. 140, A1133 (1965); R. D. Cowan, A. C. Larson, D. Liberman, J. B. Mann, and J. Waber, ibid. 144, 5 (1966). D. Liberman (private communication). We wish to thank Dr. Liberman for kindly sending us the data for the HFS field radial electron charge density. Note that in (3.1 d) we use atomic units, i.e., $m_e = \hbar = |e| = 1$.

[22]M. Abramowitz and I. A. Stegun, Handbook of Mathematical Functions (Dover, New York, 1965), p. 896. The eighth-order Adam's method, based on an eighth-order open-type Newton-Cotes predictor and an eighth-order closed-type Adam's corrector, has also been used. The Adam's method is better if the analytic expression for the potential $V(r)$ is known, such as for the point-Coulomb and the modified Thomas-Fermi model. Otherwise, the Runge-Kutta method is much better. Also, we use double precision in this work.

[23]R. H. Pratt, R. D. Levee, R. L. Pexton, and W. Aron, Phys. Rev. 134, A898 (1964).

[24]$O(x)$ shall mean the order of x.

[25]See Ref. 6; we have written a computer code to obtain the needed cases from their formulas; it was verified that this code reproduces the results which EH presented.

[26]C. D. Zerby and H. Brysk, Report No. UCC/DSSD-206, 1966 (unpublished).

[27]We have written a computer code to obtain the needed cases from the nonrelativistic formulas. It was verified that this code reproduces the nonrelativistic results without retardation calculated by Kirkpatrick and Wiedmann. There is a slight discrepancy between the results of this code and the results presented by EH for nonrelativistic theory with retardation. The nonrelativistic results given in our preliminary note (Ref. 7) are those given by EH.

[28]A. Sommerfeld and A. W. Maue, Ann. Physik 22, 629 (1935).

[29]O. Scherzer, Ann. Physik 13, 137 (1932).

[30]W. Heitler, The Quantum Theory of Radiation, 3rd ed. (Oxford U. P., London, 1954), p. 246; M. V. Mihailovic, Nuovo Cimento 9, 331 (1958).

[31]J. D. Rozics and W. R. Johnson, Phys. Rev. 135, B56 (1964). The related pair-production process has been investigated by I. Øverbø, K. J. Mork, and H. Olsen, Phys. Rev. 175, 1978 (1968). There is an inconsistency between the value a_0 given by Rozics and Johnson on p. 60 and the value a_0 calculated by integrating $I(\theta)$ over θ. The RJ results shown in Fig. 11 of the present work assume that $4\pi d\Omega_k$ of the formula for $d^3\sigma$ on p. 60 of their paper is replaced by $2d\Omega_k$.

[32]D. H. Rester and Q. Peasley (private communication).

[33]In Eqs. (4.2) and (4.3) the atomic unit is used.

[34]S. J. Biel and E. H. S. Burhop, Proc. Phys. Soc. (London) 68, A165 (1955).

[35]G. Molière, Z. Naturforsch 2a, 133 (1947).

[36]W. Heitler, Ref. 30, p. 249.

[37]H. W. Koch and J. W. Motz, Rev. Mod. Phys. 31, 920 (1959).

[38]E. Smick and P. Kirkpatrick, Phys. Rev. 60, 162 (1941); J. C. Clark and H. Kelly, ibid. 59, 220 (1941); H. Amrehn, Z. Physik 144, 529 (1956); H. Amrehn and H. Kulenkampff, ibid. 140, 452 (1955); R. Kerscher and H. Kulenkampff, ibid. 140, 632 (1955); H. Doffin and H. Kulenkampff, ibid. 148, 496 (1957); K. Bohm, Ann. Physik 33, 315 (1938); R. Honerjager, ibid. 38, 33 (1940); D. Röss, thesis, University of Würzburg, 1957 (unpublished).

[39]J. W. Motz and R. C. Placious, Phys. Rev. 109, 235 (1958).

[40]H. Mausbeck, thesis, University of Würzberg, 1957 (unpublished). H. Zeh, thesis, University of Würzberg, 1957 (unpublished).

[41]J. W. Motz, Phys. Rev. 100, 1560 (1955).

[42]N. Starfelt and H. W. Koch, Phys. Rev. 102, 1598 (1956).

[43]D. H. Rester and W. E. Dance, Phys. Rev. 161, 85 (1967).

[44]D. H. Rester, Nucl. Phys. 118, A129 (1968).

[45]H. Aiginger and H. Zinke, Acta Phys. Austriaca 23, 76 (1966).

[46]H. Aiginger, Z. Physik 197, 8 (1966).

[47]H. Aiginger (private communication). We wish to thank Dr. Aiginger for kindly sending us his recent experimental data.

[48]D. H. Rester (private communication). We wish to thank Dr. Rester for kindly sending us the results of BZRP and the experimental data.